# Investigation of the elevation of saltwater wedge due to subsurface dams

Qinpeng Chang[1,2], Tianyuan Zheng[3*], Youyuan Chen[1,2*], Xilai Zheng[1,2], Marc Walther[4,5]

1. College of Environmental Science and Engineering, Ocean University of China, Qingdao 266100, China

2. Key Laboratory of Marine Environment and Ecological Education, Ocean University of China, Qingdao 266100, China

3. College of Engineering, Ocean University of China, Qingdao 266100, China

4. Technische Universität Dresden, Faculty of Environmental Sciences, Department of Hydrosciences, Institute for Groundwater Management, Professorship for Contaminant Hydrology, 01062 Dresden, Germany

5. Helmholtz-Centre for Environmental Research–UFZ Leipzig, Department of Environmental Informatics, 04318 Leipzig, Germany

**Abstract**: Subsurface dams are rather effective and used for the prevention of saltwater intrusion (SWI) in coastal regions around the world. We carried out the laboratory experiments to investigate the elevation of saltwater wedge after the construction of subsurface dams. The elevation of saltwater wedge refers to the upward movement of the downstream saltwater wedge because the subsurface dams obstruct the regional groundwater flow and reduce the freshwater discharge. Consequently, the saltwater wedge cannot further extend in the longitudinal direction but rises in the vertical profile

* Corresponding author: Dr. Tianyuan Zheng; phone: +86-532-6678-1020; email: zhengtianyuan@ouc.edu.cn
* Corresponding author: Dr. Youyuan Chen; phone: +86-532-6678-2011; email: youyuan@ouc.edu.cn

This article has been accepted for publication and undergone full peer review but has not been through the copyediting, typesetting, pagination and proofreading process which may lead to differences between this version and the Version of Record. Please cite this article as doi: 10.1002/hyp.13863

resulting in significant downstream aquifer salinization. In order to quantitatively address this issue, field-scale numerical simulations were conducted to explore the influence of various dam heights, distances, and hydraulic gradients on the elevation of saltwater wedge. Our investigation shows that the upward movement of the saltwater wedge and its areal extension in the vertical domain of the downstream aquifer become more severe with a higher dam and performed a great dependence on the freshwater discharge. Furthermore, the increase of the hydraulic gradient and the dam distance from the sea boundary leads to a more pronounced wedge elevation. This phenomenon comes from the variation of the freshwater discharge due to the modification of dam height, location, and hydraulic gradient. Large freshwater discharge can generate greater repulsive force to restrain the elevation of saltwater wedge. These conclusions provide theoretical references for the behavior of the freshwater-seawater interface after the construction of subsurface dams and help optimize the design strategy to better utilize the coastal groundwater resources.

**Keywords**: field-scale numerical model; seawater intrusion; subsurface dam; hydraulic gradient; freshwater discharge; saltwater contaminated area; elevation of saltwater wedge; groundwater resources.

## 1. Introduction

Seawater intrusion (SWI) is a critical challenge for water management in coastal areas all over the world (Llopis-Albert & Pulido-Velazquez, 2014; Post & Werner, 2017; Kim & Yang, 2018; Zhang et al., 2019). Subsurface physical barrier and hydraulic barrier are the most effective countermeasures to prevent seawater from intruding into subsurface aquifers (Anwar, 1983; Abarca et al., 2006; Luyun

et al. 2011; Werner et al., 2013; Botero-Acosta & Donado, 2015). The long term usage of hydraulic barriers always faces the problem of clogging and water shortage in many regions (Allow, 2012). Thus, a series of impervious physical barriers are constructed to prevent SWI in Japan, Korea, China, India, the USA, the Middle East, South American, and Africa (Nawa & Miyazaki, 2009; Senthilkumar & Elango, 2011; Raju et al., 2013; Luiz et al., 2018). Physical barriers normally include subsurface dams, cutoff walls, and semi-pervious subsurface barriers (Hasan Basri, 2001; Kaleris & Ziogas, 2013; Zheng et al., 2020). Among the physical barriers, the subsurface dam is the major form in practical applications (Ishida et al., 2011). The dam height is normally set to be equal or higher than the sea level (Jamali et al., 2018; Kang & Xu, 2017; Sun et al., 2019). However, too high dams increase the construction costs, and dramatically reduce the freshwater discharge, which can lead to the accumulation of inland pollutants. Chang et al., (2019) proposed the concept of the minimum effective height to minimize the design height of the dams and enhance the freshwater discharge.

In previous studies, Sugio et al. (1987) showed that under the limiting conditions of drought and continuous groundwater mining, the cutoff wall could delay the time of SWI and inland groundwater salinization. Luyun et al. (2009) conducted experiments with subsurface dams of different heights and showed that the shorter the subsurface dam height, the faster the desalination rate of inland retained saltwater. Abdoulhalik et al. (2017) proposed a new mixed physical barrier (MPB) including a cutoff wall and a semi-permeable subsurface dam. It indicated that this combination can reduce the toe length of the saltwater wedge. Meanwhile, they investigated the effectiveness of cutoff walls for preventing SWI in layered heterogeneous aquifers (Abdoulhalik & Ahmed, 2017a). Most of the previous researches were only associated with the efficiency of preventing SWI, however, the environmental effect concerning the aquifer salinization was still insufficient. Ginkel et al., (2016) focused on

improving the recovery efficiency of the aquifer storage recovery system (ASR) with flow barriers. Their research showed that flow barriers increase recovery efficiency by preventing the stored freshwater volume from expanding sideways. But, in the long run, the upstream groundwater salinity will gradually increase and lead to soil salinization due to the interception effects of the underground dam (Cantalice et al., 2016). Abdoulhalik & Ahmed (2017b) studied the ability of subsurface dams to clean up the upstream residual saltwater, while they ignored the severe salinization of downstream aquifers after the construction of subsurface dams. Houben et al., (2018) used a flux-controlled system to study the influence of flow barriers (dykes) on groundwater flow. Their results showed the dispersive entrainment of the upstream residual saltwater generated the widening of the mixing zone, resulting in the pollution of downstream groundwater. Different from the salinization induced by the upstream residual saltwater, our research showed that the elevation of the downstream saltwater wedge after the construction of subsurface dams aggravated the aquifer salinization which can significantly influence the coastal environments.

The elevation of the freshwater-saltwater interface caused by the pumping wells (upconing) has been widely studied by researchers (Werner et al., 2013; Jakovovic et al., 2016; Abdoulhalik and Ahmed, 2018). However, the elevation of saltwater wedge induced by the subsurface dam has not been recognized and characterized, despite its importance for groundwater management in coastal areas. In this work, we explored the downstream saltwater behavior and proposed the elevation of saltwater wedge due to subsurface dams (Fig. 1). The elevation of saltwater wedge refers to the upward movement of the downstream saltwater wedge after the construction of subsurface dams. The subsurface dams obstruct the regional groundwater flow and decrease the freshwater discharge. Then the saltwater wedge cannot advance in the longitudinal direction due to the block of the dam but rises

in the vertical profile because of the reduced freshwater discharge, which eventually increases the saltwater contaminated area of the downstream aquifer. A series of tank-scale experiments and numerical simulations were conducted to prove this phenomenon and investigate the internal mechanism. The experimental results were validated very well with numerical simulations. Finally, we carried out field-scale models to understand the dependency of the elevation of saltwater wedge on the dam height, dam distance, and hydraulic gradient. According to the results of our research, the decision makers can optimize the design strategy considering the environmental influence in the coastal area.

## 2. Materials and methods

### *2.1. Experimental setup*

The laboratory experiments were carried out in a flow tank with internal dimensions of 100 cm (length) × 35 cm (height) × 5 cm (width) (Fig. 2). In order to represent a coastal aquifer, the tank with porous plates was divided into three zones in the horizontal directions, a freshwater reservoir (5 cm), a saltwater reservoir (5 cm), as well as the porous media chamber (90 cm). Glass beads with a uniform diameter of 0.7 mm were filled into the tank layer-by-layer to avoid air bubbles residing in the pores. The freshwater and saltwater reservoirs were placed at the left and right sides of the flow tank, respectively. The freshwater was pumped into the freshwater reservoir and flowed above the saltwater wedge in the porous media chamber, then overflowed through the outlet pipe in the saltwater reservoir. The constant heads of the reservoirs were controlled by drainage overflow pipes. The saltwater head was fixed at 26 cm and the freshwater head was fixed at 26.9 cm. NaCl solution with a concentration of 36 g/L was prepared as seawater. A densitometer (AlfaMirage SD-200L) was used to measure the

saltwater density $\rho_s$ = 1025 kg/m$^3$, and the freshwater density $\rho_f$ = 1000 kg/m$^3$. Cochineal dyes (red food color, Sinopharm Chemical Reagent Co., Ltd) were injected into the NaCl solution to show the movement of saltwater (Goswami & Clement, 2007). The red area in the flow tank can be recognized as the range of the saltwater wedge. The average hydraulic conductivity ($K_f$) of the porous media was determined by Darcy's experiment to be $K_f$ = 5.8 E-3 m/s, and the porosity measured by the volume method was 0.4 (Oostrtom et al., 1992). The longitudinal dispersivity was determined by fitting the breakthrough curves with a one-dimensional column test, $\alpha_L$ = 0.13 cm. The transverse dispersivity ($\alpha_T$) was assumed to be 1/10 of $\alpha_L$ in numerical simulations (Shoemaker, 2004; Lu et al, 2013). All the symbols are shown in Table 1.

A subsurface dam with a height of 16.5 cm was installed in the tank. The subsurface dam was made of impermeable plasticine, and the dam width was 1 cm for the tank-scale model. The saltwater wedge gradually formed from the sea boundary and began to invade the aquifer. The region of the saltwater wedge was recorded every 10 min using a digital camera (Canon IXUS 285 HS). When the saltwater wedge reached the subsurface dam, it continued to rise along the dam. We considered the setup achieved a dynamic equilibrium when the saltwater wedge remains stagnant for more than 10 minutes.

*2.2 Numerical models of tank- and field-scale cases*

SEAWAT was used to simulate the process of saltwater intrusion (Guo & Langevin, 2002). The tank-scale model setup and related parameters were consistent with the experiment. In addition to the tank-scale models, field-scale simulations were implemented to verify that the laboratory observations are not caused by the small tank scale and to further study quantitatively the elevation of saltwater wedge (Fig. 3). The field-scale simulation domain was 300 × 30 m$^2$. A Neumann no-flow boundary

condition was defined at the top and bottom of the domain. The left-side freshwater boundary was set to be a constant head boundary, and the constant head boundary varied in a range of 28.8-30.0 m to generate the different hydraulic gradients in numerical simulations. A constant head of 28.5 m was assigned to the right-side saltwater boundary. The concentration and density of the freshwater and saltwater were the same with those in the tank-scale model. The aquifer was assumed isotropic with an effective porosity of 0.4. The molecular diffusion coefficient ($D$) was set to 1E-9 $m^2/s$. The longitudinal dispersivity ($\alpha_L$) for the field-scale model was set to 1 m, and the transverse dispersivity ($\alpha_T$) was 1/10 of the longitudinal dispersion (Shoemaker, 2004; Lu et al, 2013). The hydraulic conductivity ($K_f$) of the aquifer and the dam was set to 6E-4 m/s and 1E-9 m/s, respectively. The dam width was 2 m for the field-scale model. Table 2 summarizes the parameter values of the field-scale models.

The tank-scale model domain was discretized into 180 × 54 quadratic elements with a grid size of 0.5 cm × 0.5 cm. The grid size and dispersivity satisfied the Péclet number criterion to ensure numerical stability (Voss & Souza, 1987):

$$Pe = \frac{v\Delta L}{D+\propto_L v} \approx \frac{\Delta L}{\propto_L} \leq 4 \quad (1)$$

where $\Delta L$ [L] is the grid size, and $D$ [$L^2/T$] is the molecular diffusion coefficient. The resulting $Pe$ = 3.8 fulfills the reporting requirements for a stable simulation. The time step was set to 60 s and the whole simulation time was set to 5 h for the tank-scale model being adequate to reach the dynamic equilibrium state. The field-scale model domain was discretized into 300 × 30 quadratic elements with a grid size of 1 m × 1 m ($Pe$ = 1). The time step was chosen to be 1 d. The whole simulation time was set to 5000 d being adequate to reach equilibrium for all testing scenarios.

Various dam heights, distances, and hydraulic gradients were set to analyze the corresponding dependency of the saltwater wedge elevation in the different scenarios of field-scale models. All the no-dam cases were set as the reference cases. The scenarios for various dam heights and distances have the same reference case whose hydraulic gradient was 3‰. The scenarios for various hydraulic gradients each have their own reference cases because various hydraulic gradients generated different saltwater wedges. All the test cases are summarized in Table 3.

*2.4 Evaluation parameters*

We defined $\Delta H$, $\Delta A$, and $\Delta M$ as the change rate of the saltwater wedge height at the dam location, the area of the downstream saltwater wedge, and the total salt mass of the downstream aquifer. These indicators were used to describe different aspects of the magnitude of the elevation of saltwater wedge. $\Delta Q$ was defined as the change of freshwater discharge induced by the construction of dams.

$$\Delta H = \frac{H_{salt} - H_{SWI}}{H_{SWI}} \tag{2}$$

$$\Delta A = \frac{A_{salt} - A_{SWI}}{A_{SWI}} \tag{3}$$

$$\Delta M = \frac{M_{salt} - M_{SWI}}{M_{SWI}} \tag{4}$$

$$\Delta Q = Q_{SWI} - Q_{salt} \tag{5}$$

where $H_{salt}$, $A_{salt}$, and $M_{salt}$ respectively represent the saltwater wedge height at the dam location, the area of the downstream saltwater wedge, and the total salt mass of the downstream aquifer in subsurface dam cases; $H_{SWI}$, $A_{SWI}$, and $M_{SWI}$ are the saltwater wedge height at the dam location, the area of the downstream saltwater wedge, and the total salt mass of the downstream aquifer (between the sea boundary and the dam location) in reference cases, respectively.

# 3 Results and discussion

*3.1. Results of tank-scale laboratory experiments and models*

Fig. 4 shows the comparison of the transient toe length (50% concentration isoline) between the laboratory and numerical results. 50% concentration isoline is commonly used to describe the saltwater wedge in the aquifer with low dispersivity (Goswami & Clement, 2007). The validation is generally well with the maximum relative difference between laboratory and numerical data 4% and 2% for the dam case and reference case. The minor discrepancies may come from the heterogeneity of glass beads. Fig. 5e provides the steady-state saltwater wedges in laboratory results showing an overall good agreement with that in numerical simulations.

Fig. 5a and 5b are photographs of laboratory experiments. We can see that the saltwater wedge height after the installation of a subsurface dam is higher than that in the reference case in Fig. 5e. This phenomenon exhibits that the saltwater wedge rises in the vertical direction due to the installed dam. The numerical simulations of the scenarios with and without dams are shown in Fig. 5c and 5d. In the reference case, the salt water advances and mixes with the fresh water in the dispersion zone. The highest freshwater velocity (5.4E-4 m/s) occurs at the outflow zone inducing by the smallest discharge area. For the dam case, the advancing seawater is obstructed at the dam location, then pushed upward in the vertical direction and mixes with the fresh water (Fig. 5d). The blockage of the dam shrinks the freshwater discharge area, and the freshwater flow above the dam speeds up significantly. The maximum freshwater velocity locates at the dam top (4.6E-4 m/s) and outflow zone (5.3E-4 m/s). The freshwater discharge in the dam case is 0.47 ml/s, and smaller than that in the reference case (0.5 ml/s).

The reduced freshwater discharge provides a less repulsive force to repel the elevation of saltwater wedge in the vertical section.

*3.2. Results of field-scale models*

Field-scale simulations were used to find out the influencing factors controlling the elevation of saltwater wedge in reality. The impacts of dam heights, dam distances, and hydraulic gradients were discussed.

*3.2.1 Various dam heights*

Fig. 6 illustrates the steady-state results of the saltwater wedge for different dam heights. We proposed the minimum effective dam height to control SWI in our previous research (Chang et al., 2019). When the dam height is lower than it, the saltwater will flow beyond the dam and form a new wedge across the dam. When the dam height is equal to or larger than it, the installed dam is able to prevent the intruding saltwater wedge. The minimum effective dam height is influenced by the dam distance from the sea and the hydraulic gradient. In this work, a series of numerical simulations were conducted to determine the minimum effective height with a given dam distance and hydraulic gradient. For the dam height of 8m, the installation of the dam cannot prevent the saltwater intrusion. The saltwater wedge extends across the dam and finally reaches a point close to the toe of the reference case. For the case of 12m dam height, the so-called minimum effective height, the dam can exactly prevent the saltwater intrusion. The saltwater wedge is slightly lower than that in the reference case. In the case that the dam is much higher (Fig. 6d), the saltwater completely occupies the downstream aquifer. It can be concluded that the minimum effective dam height achieves the lowest downstream saltwater wedge and a higher subsurface dam will result in a significant elevation of saltwater wedge leading to a large contaminated area.

In order to analyze the dependency of the dam height and the elevation of saltwater wedge, multiple simulations were conducted (Fig. 7). We found that with the increase of the dam height, the freshwater discharge first rises and then decreases (Fig. 7d). The freshwater discharge reaches the peak at the minimum effective dam height. The non-linear behavior of the relationship can be explained by the effective discharge area beyond the dispersion zone because the freshwater discharge through the effective discharge area accounts for more than 80% of the total freshwater flux in both the reference and dam cases. The vertical profile between the 10% and 90% isoline closing to the dam (vertical dispersion zone) for the reference case is 8 m, shrinks to 7.2 m for the dam height of 8 m, and reaches the smallest value of 3.6 m at the minimum effective dam height ($H_{dam}$ = 12 m). Concurrently, the size of the effective discharge area (the vertical profile between the 10% concentration isoline and the top boundary) is 12.4 m, 13.1m, and 16.6m, respectively. A high dam decreases the area of the dispersion zone by reducing the saltwater flow velocity. Smaller dispersion zone contributes to a larger effective discharge area which consequently leads to a larger freshwater discharge flux. For the cases that the dam height is larger than the minimum effective height, the high dam height is the main factor to decrease the effective discharge area resulting in the reduction of freshwater discharge.

From Fig. 7a, b, and c, We can find a general inverse ratio between $Q_{salt}$, and $H_{salt}$, $A_{salt}$, and $M_{salt}$. For the cases that dam heights are shorter than 12 m (lower than the minimum effective height), the saltwater wedge cannot be limited within the downstream aquifer. $H_{salt,}$ $A_{salt,}$ and $M_{salt}$ slightly decrease with the increase of dam height. This comes from the increase of $Q_{salt}$. For the cases that dam heights are 12 m - 28.5 m, $H_{salt,}$ $A_{salt,}$ and $M_{salt}$ increase slowly with the increase of dam height, corresponding to the reduction of $Q_{salt}$. If the dam is built higher than 28.5m, these three indicators grow rapidly. This

is because the drainage path of groundwater to the sea is completely blocked. The freshwater discharge $Q_{salt}$ is close to zero, then the downstream aquifer is occupied by the saltwater.

*3.2.2 Various dam distances*

Fig. 8 represents the results of the salinity distribution after the installation of dams at different locations. Fig. 8a shows the reference case. In Fig. 8b, c, d, the dam is constructed 10m, 50m, 90m from the sea boundary respectively. The detailed comparison of the saltwater wedge at different locations can be found in Fig. 8e. Compared with the reference case, the saltwater wedges in various dam distance cases are all raised. The elevation of saltwater wedge gradually increases with the dam distance to the sea boundary. This result clearly indicates that a farther distance of the dam leads to a more significant elevation. Meanwhile, a farther dam results in a longer saltwater wedge. The vertical rise and the longitudinal extension of the saltwater wedge together contribute to the increase of the saltwater contaminated area.

To clarify the influence of the dam distance on the elevation of saltwater wedge, multiple simulations were implemented with different distances to the sea boundary. Fig. 9 shows the influence of the dam distance on the elevation of saltwater wedge, considering the parameters of $H_{salt}$, $A_{salt}$, $M_{salt}$, and $Q_{salt}$. In Fig. 9 a, b and c, the respective curves of various dam distance cases lie all above that of the reference case, indicating that the establishment of subsurface dams induces the increase of $H_{salt}$, $A_{salt}$, and $M_{salt}$. All the freshwater discharge in dam cases is lower than that in the reference case (2.69 $m^3/d$). Furthermore, the freshwater discharge decreases gradually with the increase of the dam distance to the sea boundary (Fig. 9 d). The blue bars in Fig. 9 show the relative values of $H_{salt}$, $A_{salt}$, $M_{salt}$, and $Q_{salt}$ in contrast with the reference case. It reveals that the increase of $\Delta Q$ gradually enlarges $\Delta H$, $\Delta A$, and $\Delta M$. The prolonged dam distance generates a decrease in freshwater discharge. The reduced

freshwater discharge cannot push back the saltwater effectively, thus the elevation of saltwater wedge is more obvious.

*3.2.3 Various hydraulic gradients*

It needs to be noticed that different hydraulic gradients produce different reference cases. Larger hydraulic gradient results in a shorter and lower saltwater wedge (Fig. 10$a_1$, $b_1$, $c_1$). Meanwhile, the saltwater wedge of the dam case with a larger hydraulic gradient is generally lower than that with a smaller hydraulic gradient (Fig. 10$a_2$, $b_2$, $c_2$). This is because a large hydraulic gradient significantly rebels the saltwater intrusion regardless of the installation of dams. By comparing Fig. 10$a_1$, $a_2$, $b_1$, $b_2$, and $c_1$, $c_2$, we can also find a significant elevation of the downstream saltwater wedge after the construction of the dam. With the increase of the hydraulic gradient, the height difference of the saltwater wedge between the dam case and the reference case gradually exaggerates (Fig. 10d). This demonstrates that the same dam design with an enhanced hydraulic gradient can provoke a greater wedge elevation relative to the reference case.

Then we implemented a series of numerical tests to quantitatively explore the impact of hydraulic gradients on the elevation of saltwater wedge (see Fig. 11). From Fig. 11a, b, and c, we can find that the lines of the subsurface dam cases are always above which of the reference cases giving us the hint that the construction of subsurface dams leads to the increase of $H_{salt}$, $A_{salt}$, and $M_{salt}$. The blue bars in Fig. 11d show that the freshwater discharge of the reference cases increases much more significant than that of the dam cases with the growth of hydraulic gradient. $\Delta Q$ increases gradually and tends to have an increase of $\Delta H$, $\Delta A$, and $\Delta M$. This is because less freshwater discharge cannot push back the same amount of salt water. This phenomenon displays that the enhanced elevation of saltwater wedge is attributed to the increase in $\Delta Q$.

## 4. Summary and conclusions

The elevation of saltwater wedge after the installation of subsurface dams has been neglected for a long time, although it can lead to severe aquifer salinization. In this work, we investigated the elevation of saltwater wedge after the construction of subsurface dams through experimental and numerical methods. Our novelty and conclusions can be summarized as follows:

(1) Our investigation shows that the variation of dam height alters the freshwater effective discharge area and finally determines the freshwater flux. Large freshwater discharge can provide a greater repulsive force to restrain the elevation of the downstream saltwater wedge. The dam with the minimum effective height achieves the lowest saltwater wedge, while a higher subsurface dam results in a more significant elevation of saltwater wedge and a larger saltwater contaminated area.

(2) A farther dam leads to a greater elevation of saltwater wedge and a larger saltwater contaminated area at the same time. The elevation of saltwater wedge becomes more obvious because the increase of the dam distance leads to a reduction of freshwater discharge, and the diminished freshwater discharge is not strong enough to push back the invaded seawater. Meanwhile, a farther dam results in a longer saltwater wedge. The increase in the saltwater contaminated area is attributed to the vertical rise and the longitudinal extension of the saltwater wedge.

(3) With a larger hydraulic gradient, the elevation of saltwater wedge due to the subsurface dam is more obvious while the absolute saltwater wedge height and contaminated area after the wedge elevation were still smaller than that of the low hydraulic gradient case. Meanwhile, the freshwater discharge of the reference case increases faster than that of the dam case with the increase of the hydraulic gradient. The larger freshwater discharge difference between the reference case and the dam

case results in a more significant wedge elevation. Thus, the large hydraulic gradient is still the key to reducing the saltwater contaminated area, although it leads to a more severe elevation after the construction of subsurface dams.

To conclude, the more severe elevation of saltwater wedge is attributed to higher dams, farther dam distances, and larger hydraulic gradients, while the larger saltwater contaminated area results from higher dams, farther dam distances, and smaller hydraulic gradients. These conclusions provide theoretical references for the management of groundwater resources in the context of subsurface dams. This study firstly focused on a constant sea boundary out of simplicity. However, our empirical experience with these setups hints on the fact that temporal fluctuations of seawater levels due to tides and waves may have a significant impact on the elevation of saltwater wedge. We will investigate it in future work.

**Data Availability Statement**

The data that support the findings of this study are available from the corresponding author upon reasonable request.

**Acknowledgments**

This work was supported by the key project of Joint Foundation of NSFC-Shandong (No. U1806210), and the National Key Research and Development Program of China (No. 2016YFC0402810). We would like to thank editor Dr. David Boutt and anonymous reviewers for their comments and suggestions that helped to improve the manuscript.

**References**

Anwar H. O. (1983). The effect of a subsurface barrier on the conservation of freshwater in coastal aquifers. *Water Research*, 17(10):1257-1265. https://doi.org/10.1016/0043-1354(83)90250-6.

Abarca, E., Vazquez-Sune, E., Carrera, J., Capino, B., Desiré, G., Baatlle, F. (2006). Optimal design of measures to correct seawater intrusion. *Water Resources Research*, 42(9). https://doi.org/10.1029/2005WR004524.

Allow, K.A. (2012). The use of injection wells and a subsurface barrier in the prevention of seawater intrusion: a modelling approach. *Arabian Journal of Geosciences*, 5(5), 1151-1161. https://doi.org/10.1007/s12517-011-0304-9.

Abdoulhalik, A., Ahmed A. A., Hamill, G. A. (2017). A new physical barrier system for seawater intrusion control. *Journal of Hydrology*, 549, 416-427. https://doi.org/10.1016/j.jhydrol.2017.04.005.

Abdoulhalik, A., & Ahmed A. A. (2017a). The effectiveness of cutoff walls to control saltwater intrusion in multi-layered coastal aquifers: Experimental and numerical study. *Journal of Environmental Management*, 199, 62-73. https://doi.org/10.1016/j.jenvman.2017.05.040.

Abdoulhalik, A., & Ahmed, A. A. (2017b). How does layered heterogeneity affect the ability of subsurface dams to clean up coastal aquifers contaminated with seawater intrusion? *Journal of Hydrology*, 553, 708–721. https://doi.org/10.1016/j.jhydrol.2017.08.044.

Abdoulhalik, A., & Ahmed, A. A. (2018). Transient investigation of saltwater upconing in laboratory-scale coastal aquifer. *Estuarine, Coastal and Shelf Science*, 214 (September), 149–160. https://doi.org/10.1016/j.ecss.2018.09.024.

Botero-Acosta, A., Donado, L. D. (2015). Laboratory Scale Simulation of Hydraulic Barriers to

Seawater Intrusion in Confined Coastal Aquifers Considering the Effects of Stratification. *Procedia Environmental Sciences*, 25, 36-43. https://doi.org/10.1016/j.proenv.2015.04.006.

Cantalice, J. R. B., Piscoya, V. C., Singh, V. P., Silvia, Y.J.A.B, Barros, M. F. C. B, Guerra, S. M .S. (2016). Hydrology and water quality of a underground dam in a semiarid watershed. *African Journal of Agricultural Research*, 11(28), 2508–2518. https://doi.org/10.5897/ajar2016.11163.

Chang, Q., Zheng, T., Zheng, X., Zhang, B., Sun, Q., Walther, M. (2019). Effect of subsurface dams on saltwater intrusion and fresh groundwater discharge. *Journal of Hydrology*, 576, 508–519. https://doi.org/10.1016/j.jhydrol.2019.06.060.

Guo, W., Langevin, C. D. (2002). User's Guide to SEAWAT: A Computer Program for Simulation of Three-Dimensional Variable-Density Groundwater Flow. US Geological Survey Techniques of Water Resources Investigations 6-A7. Tallahassee, Florida.

Goswami, R. R., Clement, T. P. (2007). Laboratory-scale investigation of saltwater intrusion dynamics. *Water Resources Research*. 48, W09527. https://doi.org/10.1029/2006WR005151.

Ginkel, M. Van, Tombe, B., Olsthoorn, T., & Bakker, M. (2016). Small-Scale ASR Between Flow Barriers in a Saline Aquifer. *Groundwater*, 54(6), 840–850. https://doi.org/10.1111/gwat.12427.

Ursan Basri, M. (2001). Two new methods for optimal design of subsurface barrier to control seawater intrusion, PhD thesis, The Univ. of Manitoba.

Houben, G. J., Stoeckl, L., Mariner, K. E., & Choudhury, A. S. (2018). The influence of heterogeneity on coastal groundwater flow - physical and numerical modeling of fringing reefs, dykes and structured conductivity fields. *Advances in Water Resources*, 113(August 2017), 155–166. https://doi.org/10.1016/j.advwatres.2017.11.024.

Ishida, S., Tsuchihara, T., Yoshimoto, S., & Imaizumi, M. (2011). Sustainable use of groundwater with

underground dams. *Japan Agricultural Research Quarterly*, 45(1), 51–61. https://doi.org/10.6090/jarq.45.51

Jamali, I. A., Olofsson, B., Mörtberg, U. (2013). Locating suitable sites for the construction of subsurface dams using GIS. *Environmental Earth Sciences*, 70(6), 1-15. https://doi.org/10.1007/s12665-013-2295-1.

Kim, I. H., Yang, J. S. (2018). Prioritizing countermeasures for reducing seawater-intrusion area by considering regional characteristics using SEAWAT and a multicriteria decision-making method. *Hydrological Processes*, 32(25), 3642-3654. https://doi.org/10.1002/hyp.13283.

Jakovovic, D., Werner, A. D., Louw, P. G. B. De, Post, V. E. A., & Morgan, L. K. (2016). Advances in Water Resources Saltwater upconing zone of influence. *Advances in Water Resources*, 94, 75–86. https://doi.org/10.1016/j.advwatres.2016.05.003.

Kaleris, V. K., & Ziogas, A. I. (2013). The effect of cutoff walls on saltwater intrusion and groundwater extraction in coastal aquifers. *Journal of Hydrology*, 476, 370–383. https://doi.org/10.1016/j.jhydrol.2012.11.007

Kang, P., Xu, S. (2017). The impact of an underground cut-off wall on nutrient dynamics in groundwater in the lower Wang River watershed, China. *Isotopes in Environmental and Health Studies*, 53(1), 36–53. https://doi.org/10.1080/10256016.2016.1186670.

Luyun, R., Momii, K., Nakagawa, K. (2009). Laboratory-scale saltwater behavior due to subsurface cutoff wall. *Journal of Hydrology*, 377(3-4), 227–236. https://doi.org/10.1016/j.jhydrol.2009.08.019.

Luyun, R., Momii, K., Nakagawa, K. (2011). Effects of recharge wells and flow barriers on seawater intrusion. *Ground Water*, 49(2):239. https://doi.org/10.1111/j.1745-6584.2010.00719.x.

Lu, C., Chen, Y. Zhang, C., Luo, J. (2013). Steady-state freshwater–seawater mixing zone in stratified coastal aquifers. *Journal of Hydrology*, 505, 24-34. https://doi.org/10.1016/j.jhydrol.2013.09.017.

Llopis-Albert, C., Pulido-Velazquez, D. (2014). Discussion about the validity of sharp-interface models to deal with seawater intrusion in coastal aquifers. *Hydrological Processes*, 28(10), 3642-3654. https://doi.org/10.1002/hyp.9908.

Luiz, D. S. G. J., Vieira, F. P., Mannathal, H. V. (2018). Use of electrical resistivity tomography in selection of sites for underground dams in a semiarid region in southeastern Brazil. *Groundwater for Sustainable Development*, S2352801X17301868. https://doi.org/10.1016/j.gsd.2018.06.00.

Nawa, N., Miyazaki, K. (2009). The analysis of saltwater intrusion through Komesu underground dam and water quality management for salinity. *Paddy and Water Environment*, 7(2), 71–82. https://doi.org/10.1007/s10333-009-0154-1.

Oostrtom, M., Hayworth, J.S., Dane, J.H., Guven, O., 1992. Behavior of dense aqueous phase leachate plumes in homogeneous porous media. *Water Resources Research*, 28 (8), 2123–2134.

Post, V. E. A., Werner, A. D. (2017). Coastal aquifers: Scientific advances in the face of global environmental challenges. *Journal of Hydrology*, 551, 1-3. https://doi.org/10.1016/j.jhydrol.2017.04.046.

Raju, N. J., Reddy, T. V. K., Muniratnam, P., Gossel, W., Wycisk, P. (2013). Managed aquifer recharge (MAR) by the construction of subsurface dams in the semi-arid regions: A case study of the Kalangi river basin, Andhra Pradesh. *Journal of The Geological Society Of India*, 82(6), 657-665. https://doi.org/10.1007/s12594-013-0204-6.

Sugio, S., Nakada, K., Urish, D. W. (1987). Subsurface seawater intrusion barrier analysis. *Journal of Hydraulic Engineering*, 6(113), 767-779. https://doi.org/10.1016/0198-0254(87)91095-8.

Senthilkumar, M., Elango, L. (2011). Modelling the impact of a subsurface barrier on groundwater flow in the lower Palar River basin, southern India. *Hydrogeology Journal*, 19(4), 917-928. https://doi.org/10.1007/s10040-011-0735-0.

Shoemaker, W. B. (2004). Important observations and parameters for a salt water intrusion model. *Ground Water*, 42 (6), 829–840. https://doi.org/10.1111/j.1745-6584.2004.t01-2-.x.

Sun, Q. G., Zheng, T. Y., Zheng, X. L., Chang, Q. P. Walther, M. (2019). Influence of a subsurface cut-off wall on nitrate contamination in an unconfined aquifer. *Journal of Hydrology*, 575, 234–243. https://doi.org/10.1016/j.jhydrol.2019.05.030.

Voss, C. I., Souza, W. R. (1987). Variable density flow and solute transport simulation of regional aquifers containing a narrow freshwater-saltwater transition zone. *Water Resources Research*, 23, 1851-1866. https://doi.org/10.1029/wr023i010p01851.

Werner, A. D., Bakker, M., Post, V. E. A., Vandenbohede, A., Lu, C., Ataie-Ashtiani, B. (2013). Seawater intrusion processes, investigation and management: Recent advances and future challenges. *Advances in Water Resources*, 51, 3–26. https://doi.org/10.1016/j.advwatres.2012.03.004.

Zhang, B., Zheng, X. L., Zheng, T.Y., Xin J., Sui, S., Zhang, D. (2019). The influence of slope collapse on water exchange between a pit lake and a heterogeneous aquifer. *Frontiers of Environmental Science & Engineering*, 13(2), 20. https://doi.org/10.1007/s11783-019-1104-9.

Zheng, T., Zheng, X., Sun, Q., Wang L., & Walther, M. (2020). Insights of variable permeability full-section wall for enhanced control of seawater intrusion and nitrate contamination in unconfined aquifers. *Journal of Hydrology*, 586:124831. https://doi.org/ 10.1016/j.jhydrol.2020.124831.

**Legends**

Fig. 1. Schematic diagram of the elevation of saltwater wedge. The arrows represent the upward movement of the downstream saltwater wedge due to a higher subsurface dam (dash line).

Fig. 2. Schematic diagram of the experimental setup.

Fig. 3. Conceptual model for the numerical simulations.

Fig. 4. Comparison between the transient experimental and numerical toe length of the saltwater wedge. (a) Reference case; (b) dam case.

Fig. 5. Model validation with photographs of the (a) reference case; (b) dam case, numerical results of the (c) reference case; (d) dam case, and (e) the comparison of the saltwater wedges.

Fig. 6. Spatial salinity distribution. (a) Reference case; (b) dam case with $H_{dam}$ = 8 m; (c) dam case with $H_{dam}$ = 12 m; (d) dam case with $H_{dam}$ = 29 m; (e) comparison of 50% concentration isolines.

Fig. 7. Influence of dam heights on the downstream saltwater wedge. (a) Saltwater wedge heights at the dam location; (b) areas of the downstream saltwater wedge between the sea boundary and the dam; (c) total salt mass of the downstream aquifer between the sea boundary and the dam; (d) freshwater discharge. The lines represent $H_{salt}$, $A_{salt}$, $M_{salt}$, and $Q_{salt}$, while the bars represent $\Delta H$, $\Delta A$, $\Delta M$, and $\Delta Q$, respectively.

Fig. 8. Spatial salinity distribution. (a) Reference case; (b) dam case with $L_{dam}$ = 10 m; (c) dam case with $L_{dam}$ = 50 m; (d) dam case with $L_{dam}$ = 90 m; (e) comparison of 50% concentration isolines.

Fig. 9. Influence of dam distances on the downstream saltwater wedge. (a) Saltwater wedge heights at

the dam location; (b) areas of the down saltwater wedge between the sea boundary and the dam; (c) total salt mass of the downstream aquifer between the sea boundary and the dam; (d) freshwater discharge. The lines represent $H_{salt}$, $A_{salt}$, $M_{salt}$, and $Q_{salt}$, while the bars represent $\Delta H$, $\Delta A$, $\Delta M$, and $\Delta Q$, respectively.

Fig. 10. Spatial salinity distribution. ($a_1$) Reference case with the hydraulic gradient of 2‰; ($a_2$) dam case with hydraulic gradient of 2‰; ($b_1$) reference case with hydraulic gradient of 3‰; ($b_2$) dam case with the hydraulic gradient of 3‰; ($c_1$) reference case with the hydraulic gradient of 4‰; ($c_2$) dam case with the hydraulic gradient of 4‰; (d) comparison of 50% concentration isolines.

Fig. 11. Influence of hydraulic gradients on the downstream saltwater wedge. (a) Saltwater wedge heights at the dam location; (b) areas of the downstream saltwater wedge between the sea boundary and the dam; (c) total salt mass of the downstream aquifer between the sea boundary and the dam; (d) freshwater discharge. The lines represent $H_{salt}$, $A_{salt}$, $M_{salt}$, and $Q_{salt}$, while the bars represent $\Delta H$, $\Delta A$, $\Delta M$, and $\Delta Q$, respectively.

Table 1. List of symbols.

Table 2. Model parameters for field-scale models.

Table 3. Simulated scenarios for field-scale models.

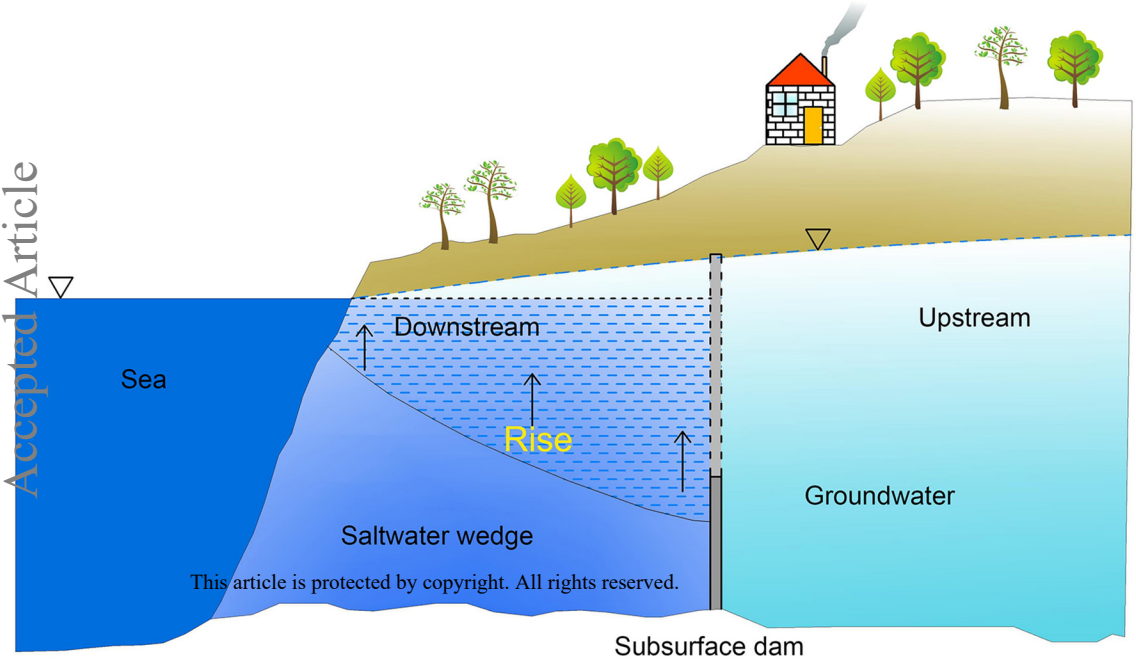

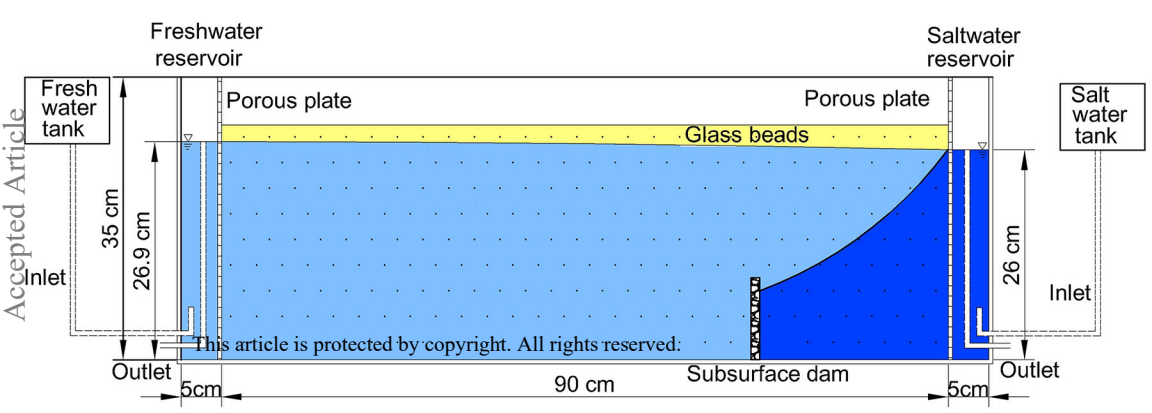

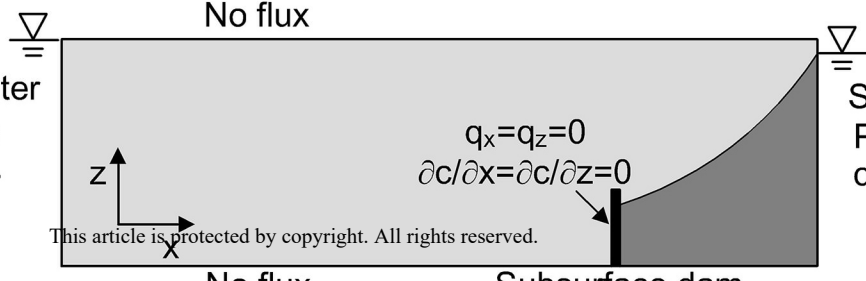

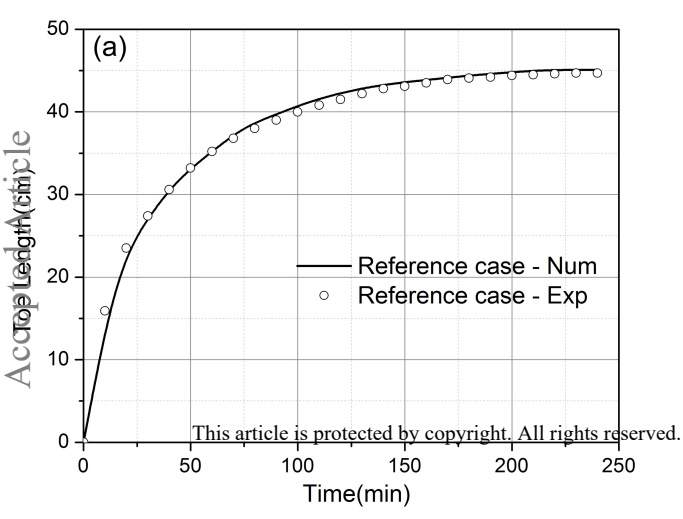




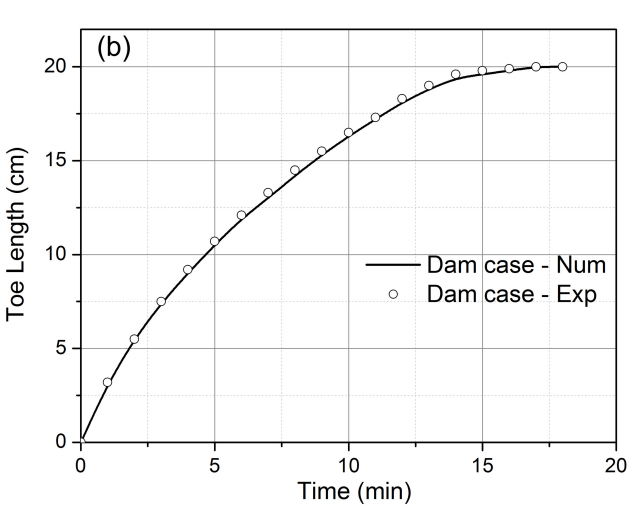

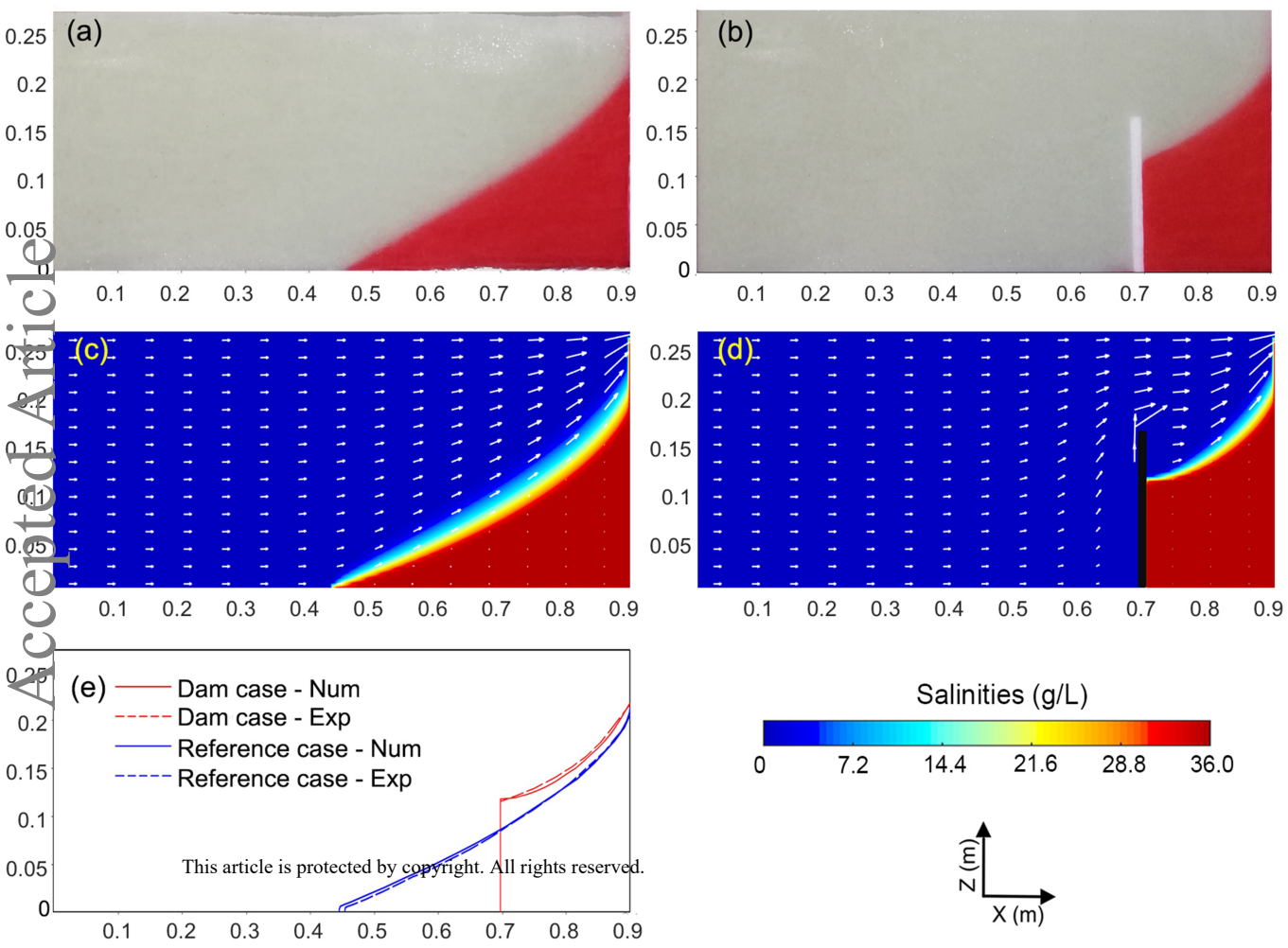

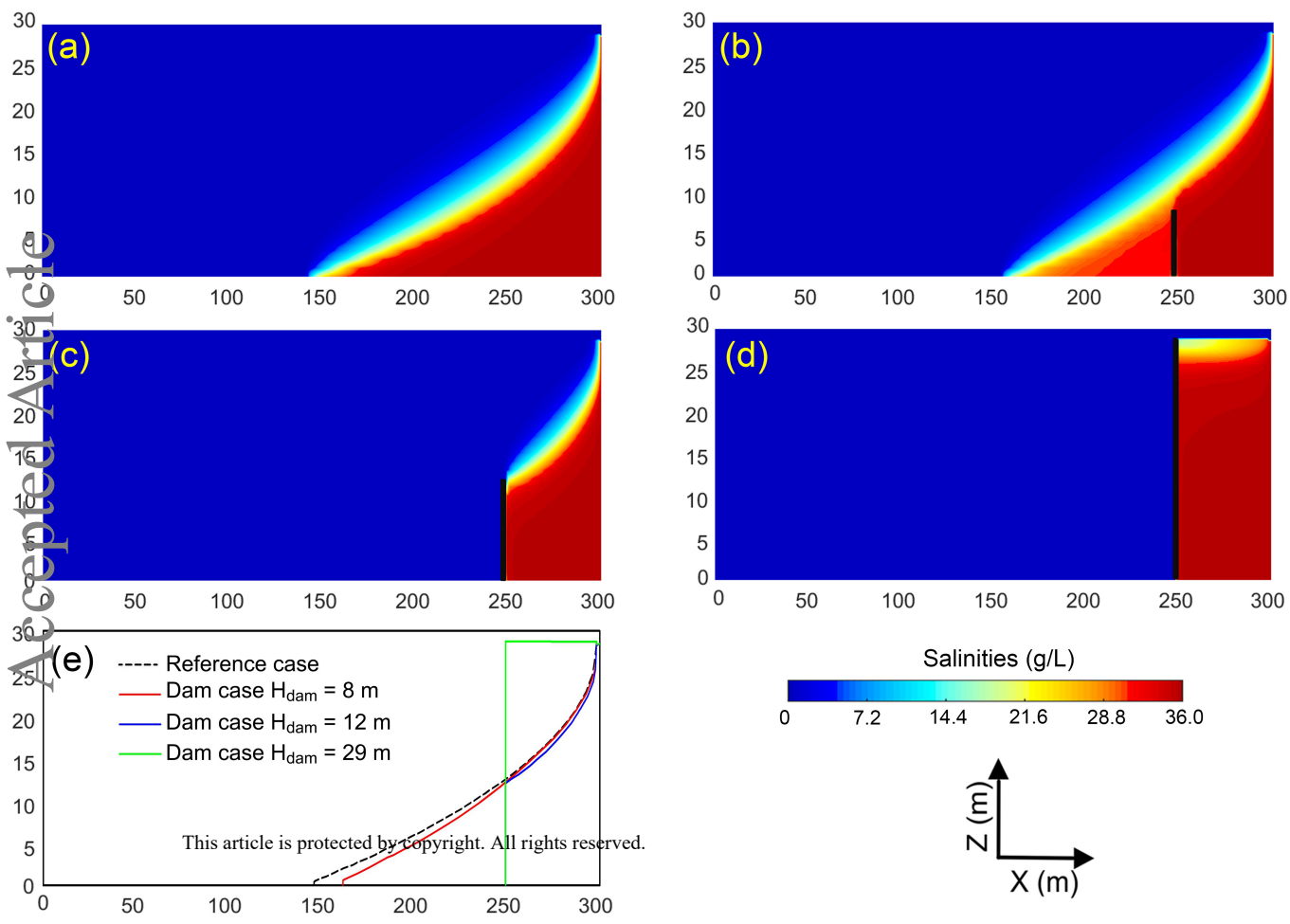

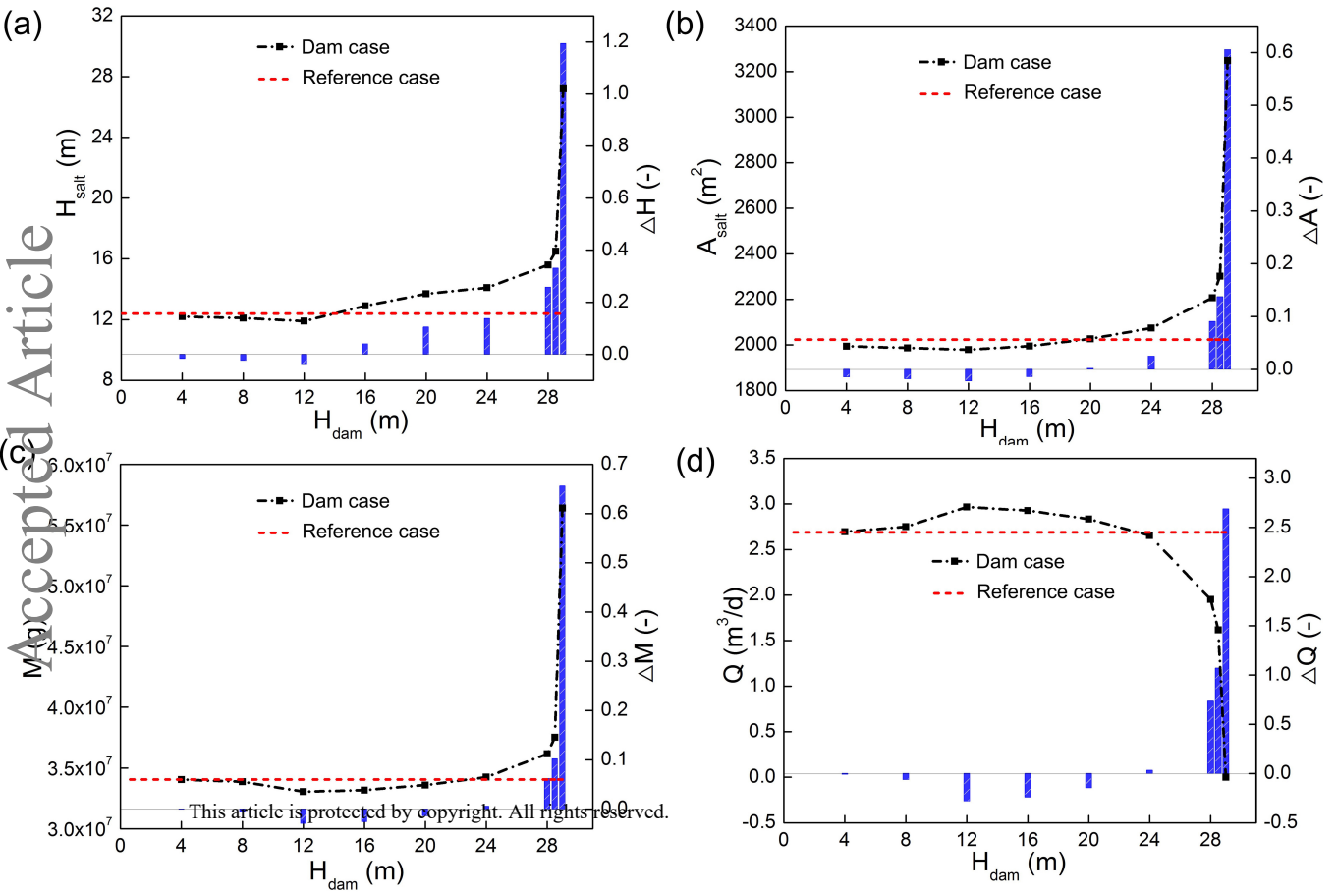

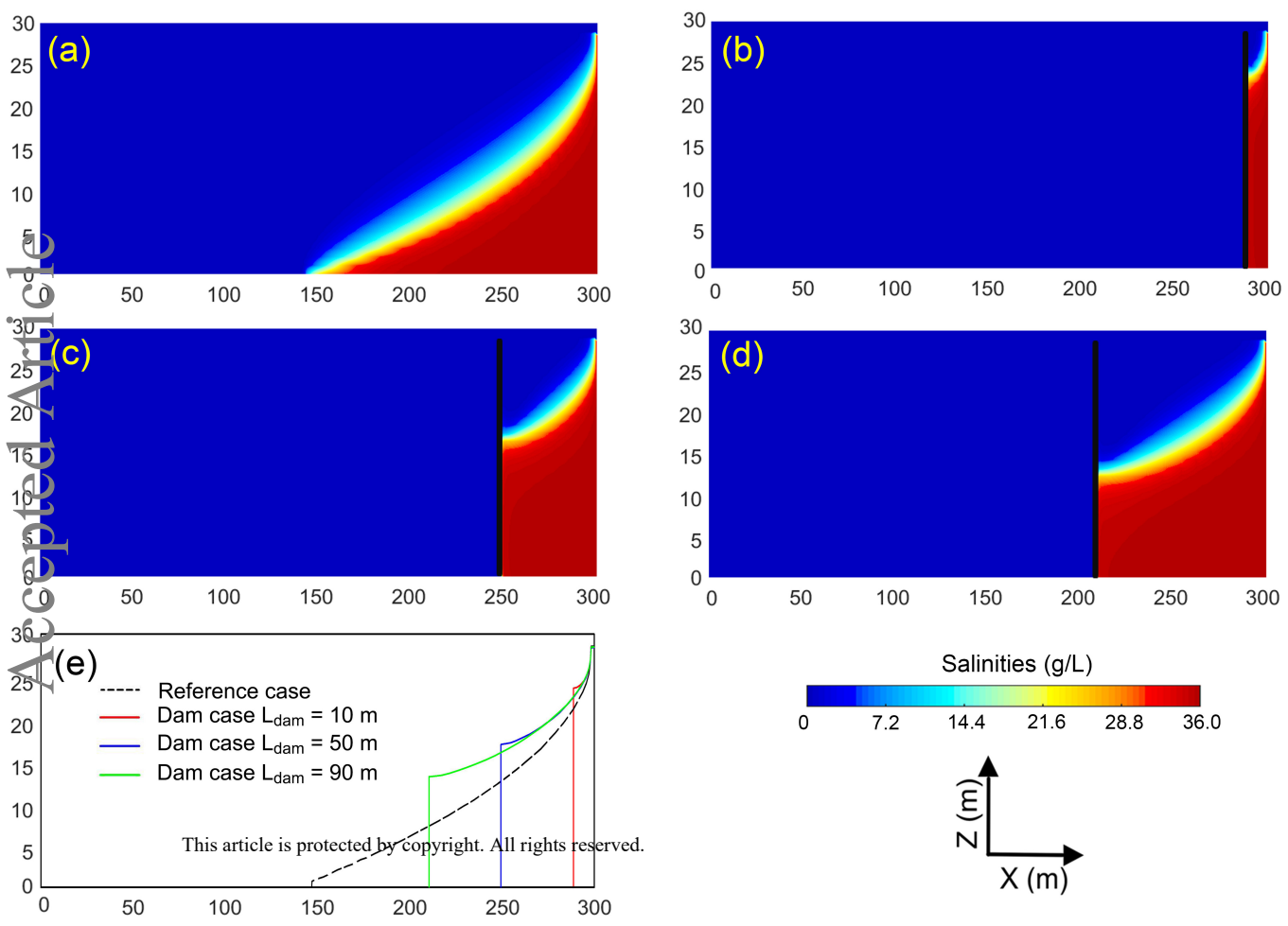

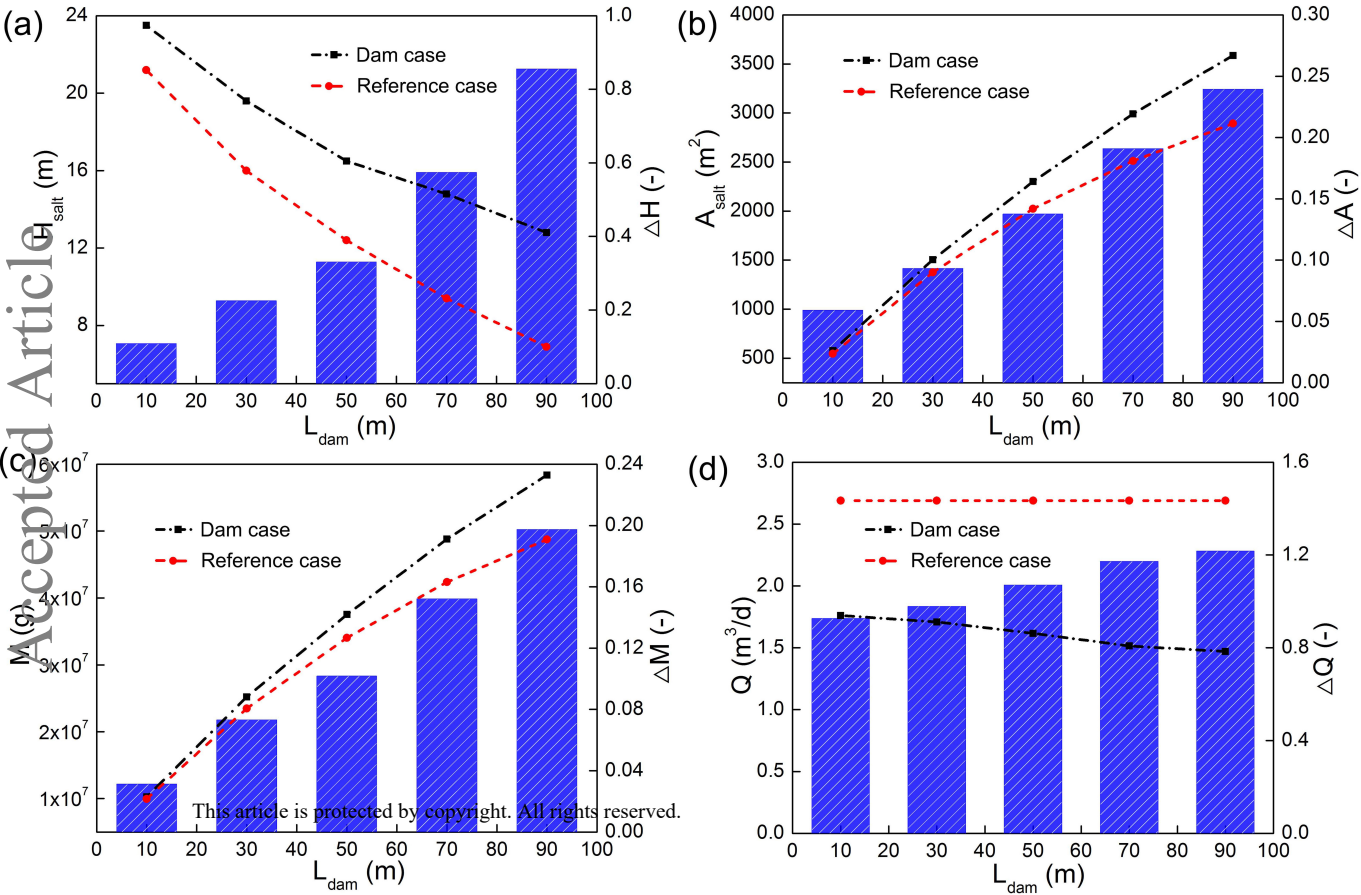

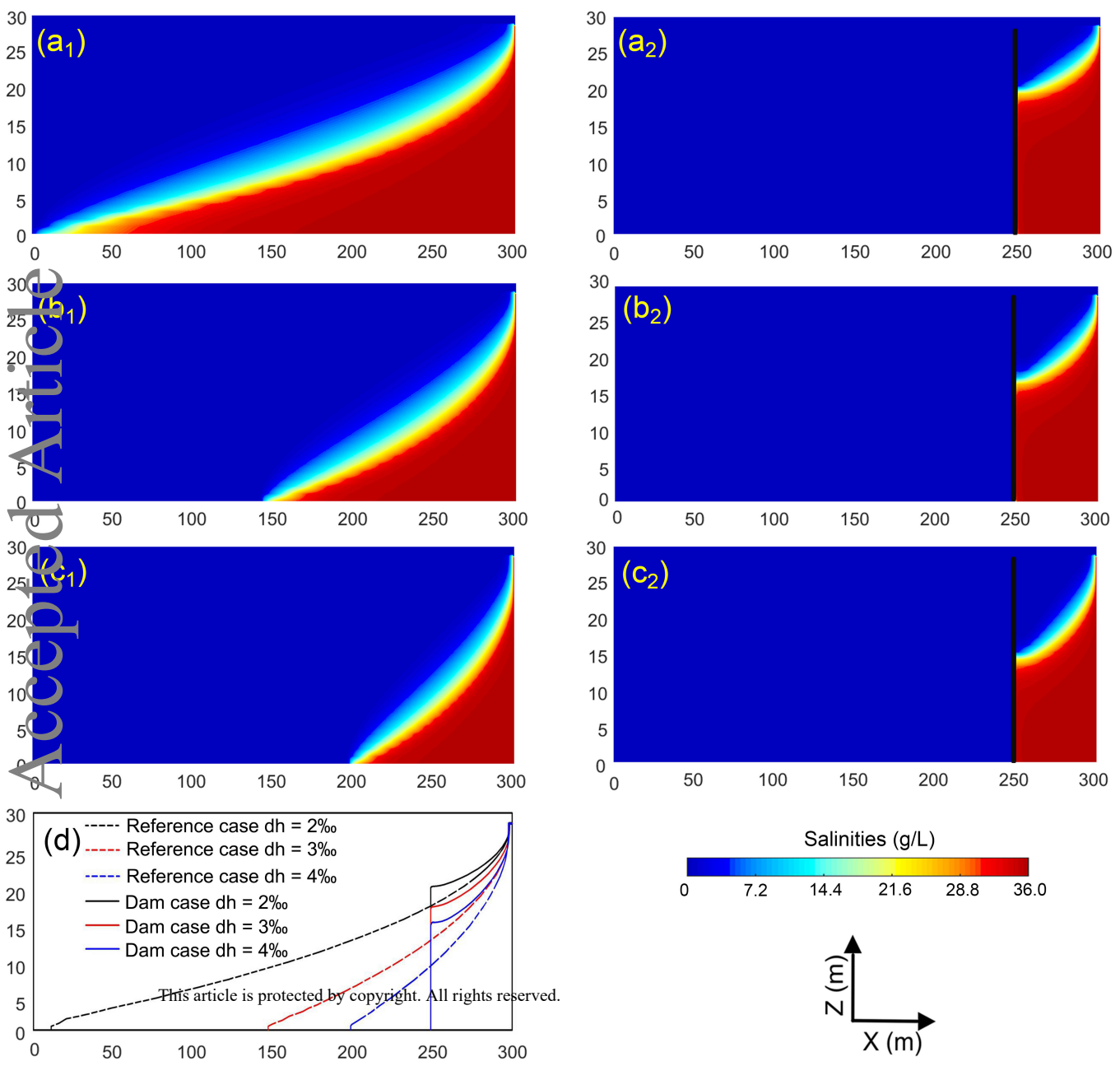

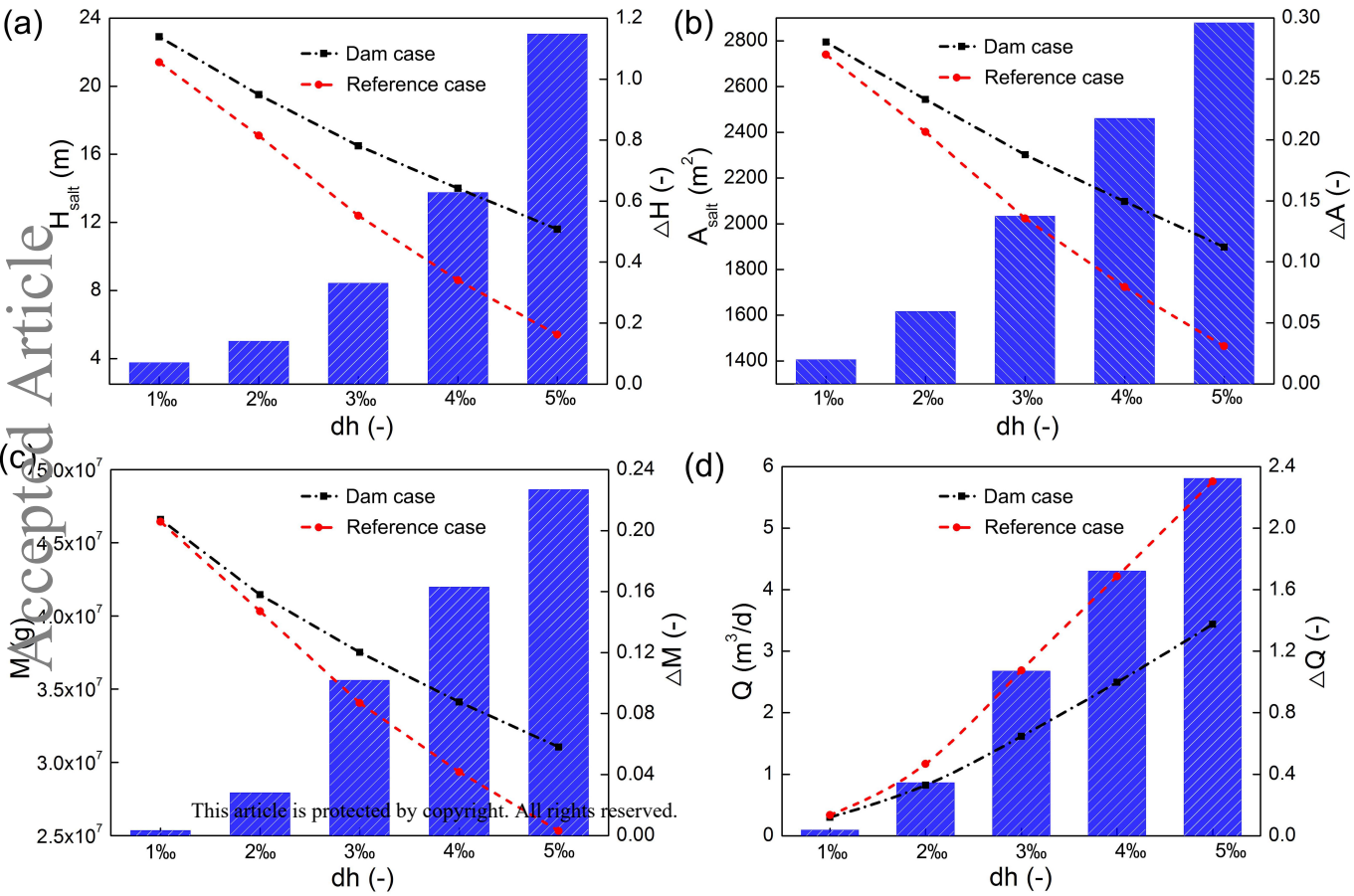

**Table 1.** List of symbols.

| | |
|---|---|
| $A_{salt}$ | area of downstream saltwater wedge (between the sea boundary and the dam location) in subsurface dam cases [$L^2$] |
| $A_{SWI}$ | area of downstream saltwater wedge (between the sea boundary and the dam location) in reference cases [$L^2$] |
| $\Delta A$ | change rate of area of downstream saltwater wedge between subsurface dam cases and reference cases [-] |
| $c_f$ | freshwater concentration [$ML^{-3}$] |
| $c_s$ | saltwater concentration [$ML^{-3}$] |
| $D$ | molecular diffusion coefficient [$L^2T^{-1}$] |
| $dh$ | hydraulic gradient [-] |
| $H_{dam}$ | subsurface dam height [L] |
| $H_{salt}$ | saltwater wedge height closing to dam in subsurface dam cases [L] |
| $H_{SWI}$ | saltwater wedge height closing to dam in reference cases [L] |
| $\Delta H$ | change rate of saltwater wedge height closing to dam between subsurface dam cases and reference cases [-] |
| $h_f$ | freshwater level [L] |
| $h_s$ | saltwater level [L] |
| $K_f$ | hydraulic conductivity [$LT^{-1}$] |
| $M_{salt}$ | total salt mass of downstream aquifer (between the sea boundary and the dam location) in subsurface dam cases [M] |
| $M_{SWI}$ | total salt mass of downstream aquifer (between the sea boundary and the dam location) in reference cases [M] |
| $\Delta M$ | change rate of total salt mass of downstream aquifer between subsurface dam cases and reference cases [-] |

| | |
|---|---|
| $Q_{salt}$ | freshwater discharge in subsurface dam cases [$L^3T^{-1}$] |
| $Q_{SWI}$ | freshwater discharge in reference cases [$L^3T^{-1}$] |
| $\Delta Q$ | difference of freshwater discharge between reference cases and subsurface dam cases [$L^3T^{-1}$] |
| $\alpha_L$ | longitudinal dispersivity [L] |
| $\alpha_T$ | transverse dispersivity [L] |
| $\rho_f$ | freshwater density [$ML^{-3}$] |
| $\rho_s$ | saltwater density [$ML^{-3}$] |

**Table 2.** Model parameters for field-scale models.

| Parameter | Unit | Value |
|---|---|---|
| Domain length | m | 300 |
| Domain height | m | 30 |
| Freshwater level ($h_f$) | m | 28.8 – 30.0 |
| Saltwater level ($h_s$) | m | 28.5 |
| Freshwater concentration ($c_f$) | g $L^{-1}$ | 0.0 |
| Saltwater concentration ($c_s$) | g $L^{-1}$ | 36.0 |
| Freshwater density ($\rho_f$) | kg $m^{-3}$ | 1000.0 |
| Saltwater density ($\rho_s$) | kg $m^{-3}$ | 1025.0 |
| Hydraulic conductivity ($K_f$) | m $s^{-1}$ | 6E-4 |
| Effective porosity ($\theta$) | - | 0.4 |
| Molecular diffusion coefficient ($D$) | $m^2$ $s^{-1}$ | 1E-9 |
| Longitudinal dispersivity ($\alpha_L$) | m | 1.0 |
| Anisotropy ratio of dispersivity ($\alpha_T$ /$\alpha_L$) | - | 0.1 |

**Table 3.** Simulated scenarios for field-scale models.

| Scenario | dam height (m) | dam distance (m) | hydraulic gradient (-) |
|---|---|---|---|
| References | - | - | 1‰, 2‰, 3‰, 4‰, 5‰ |
| Various dam heights | 4, 8, 12, 16, 20, 24, 28, 28.5, 29 | 50 | 3‰ |
| Various dam distances | 28.5 | 10, 30, 50, 70, 90 | 3‰ |
| Various hydraulic gradients | 28.5 | 50 | 1‰, 2‰, 3‰, 4‰, 5‰ |